ALTERED STRUCTURAL BRAIN NETWORK TOPOLOGY IN INFANTS WITH INTRAUTERINE GROWTH RESTRICTION

Dafnis Batalle, Elisenda Eixarch, Emma Muñoz-Moreno, Francesc Figueras, Ivan Amat-Roldan and Eduard Gratacos

Department of Maternal-Fetal Medicine,
Institut Clínic de Ginecologia, Obstetrícia i Neonatologia (ICGON), Hospital Clínic;
Institut d'Investigacions Biomèdiques August Pi i Sunyer (IDIBAPS), University of Barcelona;
Centro de investigación Biomédica en Red de Enfermedades Raras, CIBER-ER, Barcelona, Spain

ABSTRACT

Intrauterine growth restriction (IUGR) due to placental insufficiency is associated with a wide range of short- and long-term neurodevelopmental disorders. Prediction of neurodevelopmental outcomes in IUGR is among the clinical challenges of modern fetal medicine and pediatrics.
In this paper we analyze brain networks obtained from diffusion MRI of a prospective cohort of one year old infants (32 controls and 24 IUGR) and demonstrate the existence of quantifiable brain reorganization of white matter circuitry in IUGR group by means of graph theory features of brain networks. We also introduce novel graph theory measure of segregation of regional networks and apply it to our sample, finding it a useful measure to find differences in case-control studies. These findings show the potential of diffusion MRI based connectomics and graph theory based network characteristics for estimating differences in the architecture of neural circuitry.

Index Terms— Complex networks, diffusion tensor imaging, graph theory, brain modeling.

1. INTRODUCTION

IUGR due to placental insufficiency is a leading cause of fetal morbidity and mortality [1]. Prediction of neurodevelopmental outcomes in IUGR is among the clinical challenges of modern fetal medicine and pediatrics. This goal is currently hampered by the limited understanding of the brain reorganization processes leading to poor neurodevelopment in IUGR children and the lack of suitable imaging biomarkers in fetal or early life.
In recent years several studies have used magnetic resonance imaging (MRI) to demonstrate differences in brain structure and cortical development in IUGR subjects. Despite these studies are useful to demonstrate disease-related differences, the ability to use MRI information to generate individual predictive biomarkers in IUGR is limited. Connectomics [2] is an emerging approach to extract information from different modalities, including MRI data, exhaustively mapping inter-regional connectivity within the brain to build a graph model of its neural circuitry known as brain network or connectome [3], providing a framework to compare architecture of brain circuits among different individuals in a direct and elegant manner. In order to assess brain organization, graph theory tools have been proposed to allow quantifying brain network infrastructure, integration and segregation of the global functioning of a brain network [4]. Of further interest is the ability to explore regional differences by assessing graph theory characteristics of the regional networks associated to a given region.
In the present study we evaluated the hypothesis that diffusion MRI based connectomics could determine quantifiable changes resulting from the existence of brain reorganization in children who suffered IUGR. We analyzed the ability of global graph theory features of brain networks to demonstrate group differences and used regional brain network features to localize altered regional networks. In addition, we developed and tested the performance of novel exploratory graph theory measures (sub-nodal and sub-local efficiency) in order to obtain further information of regional network segregation.

2. METHODS

2.1. Subjects

A total of 56 infants at 1 year of corrected age participated in the experiment: 32 controls and 24 IUGR. Eligible IUGR cases were infants with a birth weight below the 10^{th} percentile according to local standards with any congenital and/or chromosomal defects, evidence of fetal infection or multiple monochorionic pregnancy. The study protocol was approved by the local Ethics Committee.

2.2. MRI data acquisition

Children were scanned at 12 ± 2 months corrected age (CA), during natural sleep. Structural and diffusion MRI was performed using a TIM TRIO 3.0 T MR scanner (Siemens, Germany). Diffusion images were acquired by a single-shot Echo-Planar Imaging (SE-EPI) sequence covering 30 diffusion directions with a b-value of 1000 s/mm^2 with 3-mm slice thickness with no interslice gap, 40 axial slices and in-

plane acquisition matrix of 122 x 122 with a field of view (FoV) set to 200 x 200 mm which resulted in a voxel dimension of 1.64 x 1.64 x 3 mm^3, repetition time (TR) = 9300 ms, echo time (TE) = 94ms. An additional image without diffusion weight (b = 0 s/mm^2) was also acquired. Structural T1 weighted images were obtained by a Magnetization Prepared Rapid Acquisition Gradient Echo (MPRAGE) sequence with the following parameters: 0.9-mm slice thickness with no interslice gap, 192 sagital slices, in-plane acquisition matrix of 256 x 256, FoV = 220 x 220 mm^2, which resulted in a voxel dimension of 0.86 x 0.86 x 0.9 mm^3, TR = 2050ms, TE = 2.41 ms. All acquired MRI structural and diffusion images were visually inspected for apparent or aberrant artifacts. Additional T2 weighted volume was also acquired in order to exclude WM abnormalities. Diffusion images were corrected for eddy currents effects using FMRIB's Diffusion Toolbox (FSL 4.1).

2.4. Network construction

2.4.1. White matter and grey matter segmentation

Structural volumes were segmented into WM, grey matter (GM) and cerebrospinal fluid (CSF) using SPM8 toolbox. Since the software package uses default tissue probability maps derived from adult brains, we replaced the original tissue probability maps by specific one year old infant ones [5] which could fit better with the anatomical brain features of the patients included in the study. Structural volume of each subject was registered to its correspondent b_0 volume (in the diffusion native space) using IRTK software to perform a 3D voxel-based affine registration [6]. The transformation obtained for each subject was also used to transform WM, GM and CSF to the diffusion native space.

2.4.2. Network node definition

Automated brain parcellation was achieved by reproducing the methods for a two-year-old cohort performed successfully in 33 subjects by Gousias et al. [7]. We normalized each of Gousias' atlases using unified segmentation model [8] with the same tissue probability maps used in previous step [5]. To avoid some issues with small regions, we merged some of the 83 ROIs described by Gousias' into 59 ROIs according to an anatomical-functional criterion. We used a vote-rule based decision fusion procedure to combine the information of the multiple individual labeled atlases in a single template from the 33 subject-specific atlases. The labels of this template were elastically propagated to each of our subjects structural MRI acquisitions using the inverse normalization transformation obtained with the previous unified segmentation step [8], and transformed to diffusion native space with the previously calculated affine transformation. Discrete labeling values were preserved by nearest neighbor interpolation for both transformations.

2.4.3. WM Tractography

A deterministic tractography was performed for each subject diffusion data using a diffusion tensor imaging (DTI) based fiber tracking algorithm with log-euclidean metrics [9], available on MedINRIA 1.9 software.

2.3.4. Network edge definition

Tractography generated in the previous step was integrated to the anatomical parcellation in diffusion space in order to construct an inter-cortical brain binary network. Two nodes (regions) *i* and *j* were considered to be connected by an edge e_{ij}, when there exist at least one fiber bundle *f* with end-points in *i* and *j* WM-GM interface. Some authors have proposed to establish a threshold of a minimum number of fiber bundles connecting two ROIs to consider them connected by an edge. However, it has been demonstrated that the use of different thresholds does not significantly influence the resulting network analysis in case-control studies [10-11]. Therefore, we applied an unthresholded binary network criterion in order to preserve the whole structure of the connectivity in each individual.

2.5. Network analysis

Brain networks were characterized at two levels: global and regional. At a global level, network infrastructure (i.e. mean degree), segregation (i.e. local efficiency) and integration (i.e. global efficiency) were characterized. At a regional level network infrastructure (i.e., nodal degree) and regional network integration (i.e., nodal efficiency) were assessed [4]. In this study the inclusion of a further level of analysis was explored, based on the idea of introducing regional network segregation. Firstly, one additional characteristic to the regional analysis was included, a regional measure of brain networks that was named 'sub-nodal efficiency', which assesses regional network segregation by computing the local efficiency of each regional network:

$$E_{sub-nodal}(i) = \frac{1}{k_i} \sum_{j \in N_i} \left(\frac{1}{k_j^i \left(k_j^i - 1 \right)} \sum_{h,l \in N_i, [h,l] \neq j} a_{jh} a_{jl} \left[d_{hl}(N_i^j) \right]^{-1} \right)$$

Where k_j^i is the degree of node *j* in the regional network N_i, and $d_{hl}(N_i^j)$ is the shortest path length between nodes *h* and *l* that contains only neighbors of node *i* that are also neighbors of *j*. Given a network of a subject, a regional network associated to a given node was defined as the new network composed by the neighbors of that node, that is, by the nodes that are connected to that node. Nodes *i* and *j* are considered neighbors in a network if there exist an edge e_{ij} that connect both nodes [4]. Secondly, in a similar way to the existing relationship between nodal and local efficiency, sub-nodal efficiency naturally provided a novel global parameter based on its averaged value onto the network that was analogously named 'sub-local efficiency':

$$E_{sub-local} = \frac{1}{n}\sum_{i\in N} E_{sub-nodal}(i) = \frac{1}{n}\sum_{i\in N}\left(\frac{1}{k_i}\sum_{j\in N_i}\left(\frac{1}{k_j^i\left(k_j^i-1\right)}\sum_{h,l\in N_i,[h,l]\neq j} a_{jh}a_{jl}\left[d_{hl}(N_i^j)\right]^{-1}\right)\right)$$

Where N is the set of nodes in the network and n its cardinal. In a similar way as local efficiency of a network is defined as the average global efficiency of each regional network, sub-local efficiency was defined as the average local efficiency of each regional network. This computation resulted in a second order measure of the segregation of the whole network, as it was defined as the average segregation measure of each regional network.

2.6 Statistical analysis

Statistical comparisons among groups were performed by general linear models with gender, maternal education level, smoking during pregnancy and breastfeeding as cofactors and gestational age as a covariate. Due to the exploratory nature of these analyses, significance was declared at $p<0.05$ (uncorrected). The software package SPSS 18.0 (SPSS, Chicago, IL) was used for the statistical analyses. All computational algorithms were implemented using MATLAB (2007b, The MathWorks Inc., Natick, MA).

3. RESULTS AND DISCUSSION

3.1 General connectivity characteristics

Graph theoretical analysis on the adjacency matrices representing structural brain networks of our subjects, showed that 1-year old children structural brain networks are a small-world network of neural tracts. The comparison among local and global efficiencies of the structural brain networks and its random and lattice equivalents showed that all our population fulfilled a small-world criterion, having an intermediate global and local efficiency compared to its random and regular equivalent networks (Fig. 2A and 2B). In addition, an analysis of the network cost of both groups, showed no significant differences between groups (Fig 2C).

3.3 Global connectivity characteristics

General linear models showed that children at one year of age with IUGR presented a significantly lower local efficiency of structural brain network compared with controls (group effect: F=6.093 p=0.019, Fig. 3C). Sub-local efficiency was also significantly lower in IUGR group (group effect: F=8.398 p=0.007, Fig. 3D). Interestingly, sub-local efficiency maximizes the difference between both groups. However, average degree and global efficiency were not significantly different among groups (Fig. 3A and 3B).
The lack of significant changes in mean degree or global efficiency network features between IUGR and control group is indicative of similar network in terms of infrastructure and integration. However, we could find significant changes at a second level of complexity, local efficiency, which averages the alterations in regional networks. A third level of scale was explored, by assessing sub-local efficiency of brain networks, which was also significantly lower for IUGR children. This measure is much related with the segregation of regional networks, hence, being a second order measure of segregation of the whole brain network.

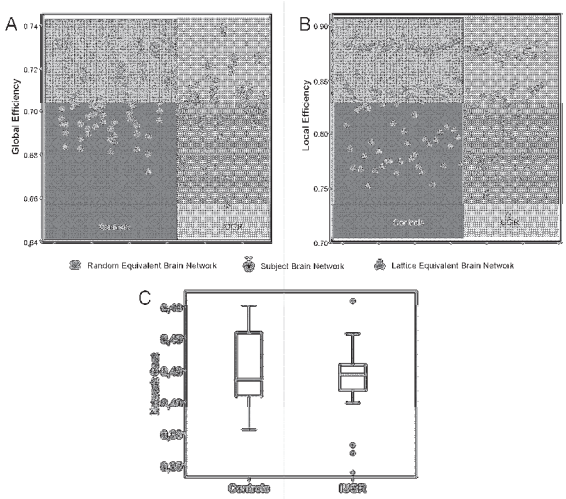


Figure 1. A) Global Efficiency and B) Local Efficiency of each subject compared with an equivalent random and lattice network with the same degree distribution. C) Network cost of controls and IUGR.

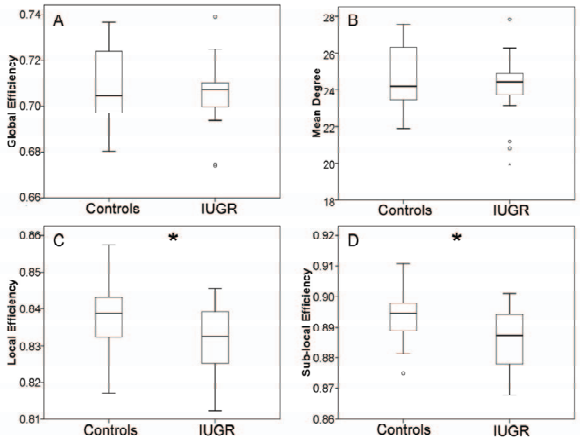


Figure 2. Control and IUGR brain network global characteristics: A) global Efficiency, B) mean degree, C) local efficiency and D) sub-local efficiency.

3.4 Regional connectivity characteristics

Further analysis of regional connectivity revealed statistically significant differences at a regional level on the set of features evaluated (Fig. 4). Nodal network infrastructure, assessed by nodal degree, was altered in right inferiolateral remainder of parietal lobe, right postcentral gyrus and right superior parietal gyrus. Interestingly, previous studies have linked worst motor performance with reduced GM in parietal areas of IUGR [12]. Functional integration of regional networks, assessed by means of nodal

efficiency, was altered in IUGR for left superior temporal gyrus, left middle frontal gyrus, right thalamus, right precentral gyrus, right postcentral gyrus, left lingual gyrus and right cuneus. Several studies have previously reported alterations in frontal and temporal areas, involved in the regulation of cognitive functions previously reported to be abnormal in IUGR children [13-14]. Functional segregation of regional sub-networks, assessed by means of sub-nodal efficiency, was disrupted at right and left superior temporal gyrus, right and left middle and inferior temporal gyrus, brainstem, left insula, left middle frontal gyrus, right and left striatum, right and left thalamus, right precentral gyrus, right anterior and medial orbital gyrus, left lingual gyrus and right cuneus. Interestingly, by means of sub-local efficiency differences on insular cortex, striatum and thalamus were also found. Previous studies have revealed relative reduction of insular lobe GM and WM volumes in IUGR children [12] and alterations in the cortico-striato-thalamic network have been associated with several cognitive disorders [15].

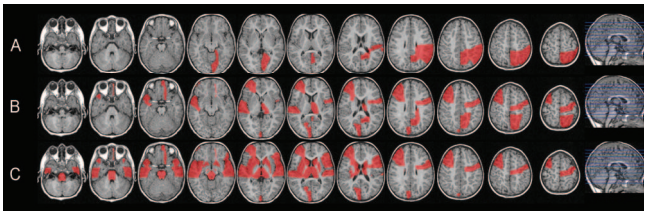


Figure 3. Altered regional features in IUGR. In red, regional characteristics showing statistically significant differences in IUGR compared with controls. (A) Nodal degree, (B) nodal efficiency and (C) sub-nodal efficiency.

4. CONCLUSION

MRI connectomics is suitable for the assessment of brain reorganization in IUGR infants by means of global and regional graph theory based network features. We could demonstrate altered brain network topology in one-year-old IUGR infants by means of global graph theory features, and localize an altered pattern of regional features. The findings show the potential of diffusion MRI based connectomics and graph theory based network analysis for extracting features that characterize the individual architecture of neural circuitry. The use of novel sub-local efficiency measure allowed to better separate case and control groups, suggesting that it could be a useful tool in case-control studies. In addition novel sub-nodal efficiency measure allowed identifying a set of altered regional networks not identified with other regional graph theory measures. This technique stands as a good candidate for the development of imaging biomarkers of poor neurodevelopmental outcome in infants at risk due to prenatal diseases.

4. ACKNOWLEDGMENTS

This work was supported by La Caixa Foundation, Barcelona, Spain; The Cerebra Foundation for the Brain-Injured Child, Carmarthen, Wales, UK; The Thrasher Research Fund, Salt Lake City, USA; grants from Carlos III Institute of Health, Spain (CM08/00105 to E.E and CD11/00048 to E.M.) and Marie Curie IAPP (FP7-PEOPLE-2007-3-1-IAPP 217911 uVOLUMES, to I.A.). IRTK was used under Licence from Ixico Ltd.

5. REFERENCES

[1] S. Jarvis, S.V. Glinianaia, M.G. Torrioli, M.J. Platt, M. Miceli, P.S. Jouk, A. Johnson, J. Hutton, K. Hemming, G. Hagberg, H. Dolk, and J. Chalmers, "Cerebral palsy and intrauterine growth in single births: European collaborative study," *Lancet,* vol. 362, pp. 1106-11, 2003.

[2] P. Hagmann, "From diffusion MRI to brain connectomics.," Lausane: Signal Processing Institute. Ecole Polytechnique Fédérale de Lausanne (EPFL), 2005.

[3] O. Sporns, G. Tononi, and R. Kotter, "The human connectome: A structural description of the human brain," *PLoS Comput Biol,* vol. 1, p. e42, 2005.

[4] M. Rubinov and O. Sporns, "Complex network measures of brain connectivity: uses and interpretations," *Neuroimage,* vol. 52, pp. 1059-69, 2009.

[5] M. Altaye, S.K. Holland, M. Wilke, and C. Gaser, "Infant brain probability templates for MRI segmentation and normalization," *NeuroImage,* vol. 43, pp. 721-30, 2008.

[6] C. Studholme, D.L.G. Hill, and D.J. Hawkes, "An overlap invariant entropy measure of 3D medical image alignment," *Pattern Recognition,* vol. 32, pp. 71-86, 1999.

[7] I.S. Gousias, D. Rueckert, R.A. Heckemann, L.E. Dyet, J.P. Boardman, A.D. Edwards, and A. Hammers, "Automatic segmentation of brain MRIs of 2-year-olds into 83 regions of interest," *NeuroImage,* vol. 40, pp. 672-84, 2008.

[8] J. Ashburner and K.J. Friston, "Unified segmentation," *Neuroimage,* vol. 26, pp. 839-51, 2005.

[9] P. Fillard, X. Pennec, V. Arsigny, and N. Ayache, "Clinical DT-MRI estimation, smoothing, and fiber tracking with log-Euclidean metrics," *IEEE Transactions on Medical Imaging,* vol. 26, pp. 1472-1482, 2007.

[10] N. Shu, Y. Liu, K. Li, Y. Duan, J. Wang, C. Yu, H. Dong, J. Ye, and Y. He, "Diffusion tensor tractography reveals disrupted topological efficiency in white matter structural networks in multiple sclerosis," *Cereb Cortex,* vol. 21, pp. 2565-77, 2011.

[11] Y. Li, Y. Liu, J. Li, W. Qin, K. Li, C. Yu, and T. Jiang, "Brain anatomical network and intelligence," *PLoS Comput Biol,* vol. 5, p. e1000395, 2009.

[12] N. Padilla, C. Falcon, M. Sanz-Cortes, F. Figueras, N. Bargallo, F. Crispi, E. Eixarch, A. Arranz, F. Botet, and E. Gratacos, "Differential effects of intrauterine growth restriction on brain structure and development in preterm infants: a magnetic resonance imaging study," *Brain Res,* vol. 1382, pp. 98-108, 2011.

[13] R. Geva, R. Eshel, Y. Leitner, A. Fattal-Valevski, and S. Harel, "Memory functions of children born with asymmetric intrauterine growth restriction," *Brain Res,* vol. 1117, pp. 186-94, 2006.

[14] E. Eixarch, E. Meler, A. Iraola, M. Illa, F. Crispi, E. Hernandez-Andrade, E. Gratacos, and F. Figueras, "Neurodevelopmental outcome in 2-year-old infants who were small-for-gestational age term fetuses with cerebral blood flow redistribution," *Ultrasound Obstet Gynecol,* vol. 32, pp. 894-9, 2008.

[15] S.V. Faraone and J. Biederman, "Neurobiology of attention-deficit hyperactivity disorder," *Biol Psychiatry,* vol. 44, pp. 951-8, 1998.